J. Fluid Mech. (1984), *vol.* 143, *pp.* 253–276
Printed in Great Britain

The dynamics of stretched vortices

By JOHN C. NEU
Mathematical Sciences Research Institute, 2223 Fulton Street, Room 603, Berkeley, CA94720

(Received 18 January 1983 and in revised form 30 May 1983)

The dynamics of vortices subject to stretching by a uniform plane straining flow is studied asymptotically and by means of a new class of exact solutions. The asymptotic analysis treats the stretched Burger's vortex sheet for strain rates much greater than the gradient of the sheet strength. It is found that portions of the sheet where the strength density is sufficiently large compared to (viscosity × strain rate)$^{\frac{1}{2}}$ will collapse to form concentrated vortices. The exact solutions describe uniform vortices of elliptical cross-section in inviscid fluid subject to stretching parallel to their axes. These solutions complement the description of vortex collapse found by asymptotic methods. The relevance of these results stems from the prevalence of vortex structures subject to strain in turbulent flows.

1. Introduction

A problem of great current interest in fluid mechanics is to describe and interpret the evolution of vortical structures in the mixing layer (Browand & Winant 1974; Brown & Roshko 1974; Browand & Weidman 1976; Roshko 1976; Saffman & Baker 1979). A descriptive theory of Corcos (Corcos & Sherman 1984; Corcos & Lin 1984; Lin & Corcos 1984) based on his interpretation of well-known experiments (Browand & Winant 1974; Brown & Roshko 1974; Browand & Weidman 1976; Roshko 1976) and extensive numerical simulations gives caricatures of the most important vortex motions. The basic flow is two-dimensional, consisting of the rollup and pairing of large spanwise vortices whose axes are perpendicular to the streamwise direction. Figure 1 depicts schematically two neighbouring vortices in an array produced by the rollup process. The large spanwise rolls are connected by filaments called braids. The braids are subjected to strain produced by the rolls, so that spanwise vorticity is withdrawn from the braids and transferred to the rolls. The streamlines drawn in figure 1 illustrate graphically this effect of the roll-induced strain.

The basic system of rolls and braids forms a background flow for various secondary vortices. The streamwise streaks observed in the braids (Corcos & Sherman 1984; Corcos & Lin 1984; Lin & Corcos 1984) are due to arrays of alternating vortices whose axes follow the braids in the streamwise direction. These are depicted schematically in figure 2. The formation of these secondary vortices is bound up with the development of the large spanwise rolls from an initially parallel shear flow. Hence an array of secondary vortices has wavelength λ comparable to the spacing L between rolls produced from Kelvin–Helmholtz instability of parallel shear flow. The strain tends to compress secondary vortices into the planes of the braids, but this is resisted by viscous diffusion. The thickness of secondary vortices determined by the balance between these two opposing effects is $\delta \equiv (\pi\nu/2\gamma)^{\frac{1}{2}}$, where ν is the kinematic viscosity and γ is the strain rate. Since the strain in the braids is due to the larger spanwise rolls, the strain rate γ should be $O(\Delta U/L)$, where ΔU is the total shear across the

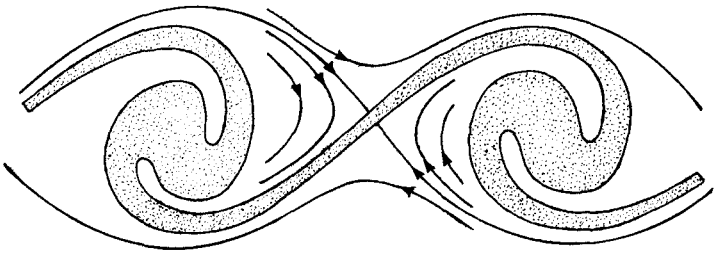

FIGURE 1. The rollup of spanwise vortices.

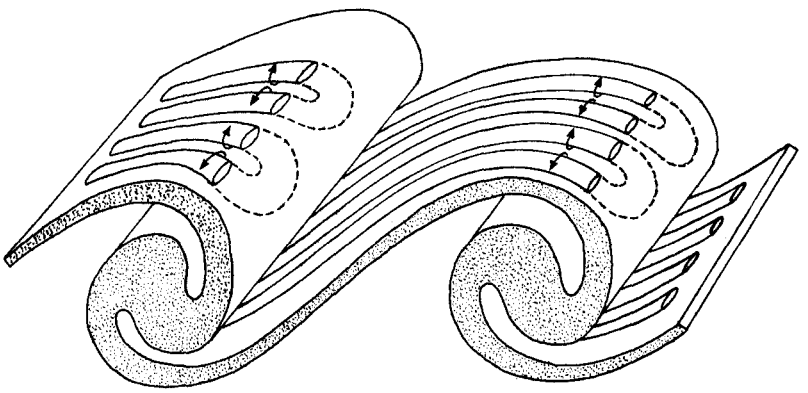

FIGURE 2. The streamwise streaks in the braids.

mixing layer. From the preceding estimates for the initial dimensions of secondary vortices and the magnitude of the strain that acts upon them, we find that their aspect ratio $a \equiv \lambda/\delta$ is $O(Re^{\frac{1}{2}})$, where $Re \equiv \Delta UL/\nu$ is the Reynolds number that characterizes the basic two-dimensional flow. We see that, for high Reynolds numbers, the secondary vortices initially appear as the highly flattened ribbons depicted in figure 2.

Under these conditions, an additional mode of vortex motion may appear. Locally, a highly flattened secondary vortex looks like a shear layer whose vortex lines are stretched by the strain. If the shear layer is sufficiently strong, it may exhibit miniature versions of the same processes observed in the basic two-dimensional flow, including the growth of concentrated rolls and their pairwise coalescence.

In this paper we present an analytical theory for the evolution of secondary vortices and their instabilities of the basis of a model due to Corcos and Lin (Corcos & Lin 1984; Lin & Corcos 1984). In §2 we give a brief description of their model and the results of numerical simulations based upon it. Certain of the simulations demonstrate a dramatic collapse of initially flattened secondary vortices into concentrated circular vortices. We review in detail their qualitative account of the collapse mechanism. In §3 we formulate the model of Corcos and Lin in the language of vortex dynamics. From this point of view, the model describes the dynamics of parallel vortices stretched by a uniform plane strain. In §4 we present the theory of stretched vortices in ideal fluid. This includes an asymptotic theory and a new class of exact solutions. Both dramatically demonstrate the collapse mechanism presented qualitatively by Corcos and Lin. In §5 we present a simple heuristic theory of stretched vortices in viscous fluid. The essential change from the inviscid case is that viscous diffusion of vorticity creates a limited resistance against the collapse. We apply the viscous theory to the collapse of secondary vortices, and determine a criterion for the collapse of

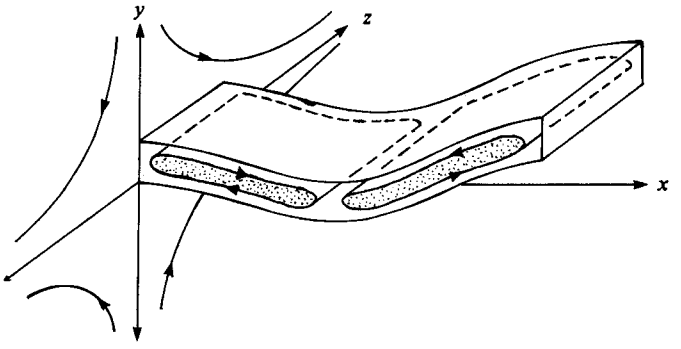

FIGURE 3. The physical situation of the model problem.

initially flattened secondary vortices into concentated vortices. The equations of the heuristic theory used here are ill-posed with respect to certain classes of initial conditions. In §6 we present the asymptotic analysis that yields the heuristic theory at leading order plus higher-order corrections that restore the well-posedness. In §7 we use the extended theory to discuss the Kelvin–Helmholtz instability of the Burgers vortex sheet. In §8 we present an asymptotic theory of the strong, nearly circular vortices that appear in the final stage of the collapse process. The solutions found here are closely related to the well-known Burger's vortex.

2. The model and its phenomenology

In the advanced stages of the basic two-dimensional rollup induced by Kelvin–Helmholtz instability, most of the spanwise vorticity is depleted from the centres of the braids and the axes of the remaining secondary vortices are all aligned in the principal direction of the strain created by the large spanwise rolls. Accordingly, Corcos & Lin (1984) and Lin & Corcos (1984) study the dynamics of vortices whose axes are straight lines parallel to the principal axis of a uniform plane straining flow. Figure 3 depicts the physical situation of the model problem. The streamlines drawn in the (y,z)-plane are those of the uniform plane straining flow. These streamlines are the same in each plane parallel to the (y,z)-plane. The vortices are all aligned in the z-direction, which corresponds to the principal axis of the uniform plane strain. We see that the vortices are continually stretched by the action of the strain. In this sense, we are studying the dynamics of stretched vortices.

Corcos and Lin study the evolution of vortices in the model problem by numerical integration of the Navier–Stokes equations. For a simulation of secondary vortices, the initial condition is taken to be an array of alternating vortices with wavelength λ and circulation Γ per vortex. Figure 4(a) shows a typical initial configuration. The subsequent evolution is determined by the values of the aspect ratio $a \equiv \lambda/\delta$ and the non-dimensionalized circulation $\Gamma^* \equiv \Gamma/8\gamma\lambda^2$. Since the main interest is in high-Reynolds-number flows, the aspect ratio is typically large. The numerical computations show that, for a given value of the aspect ratio, an array of alternating vortices with sufficiently weak circulation will undergo slow decay due to interdiffusion of positive and negative vorticity, whereas sufficiently strong vortices will buckle and collapse into concentrated circular vortices of radius $O(\delta)$. Figures 4(a–c) are a sequence of snapshots from a numerical simulation showing how the vorticity contours evolve during such a collapse.

From the examination of their numerical results, Corcos and Lin propose a

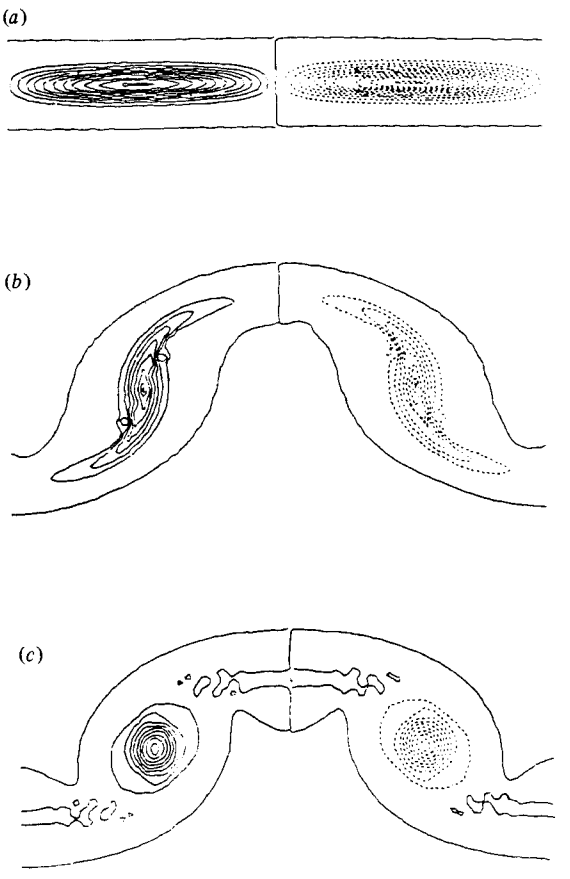

FIGURE 4. The collapse of secondary vortices.

qualitative theory of the collapse. As is evident from figures 4(*a*, *b*), the flattened secondary vortices tend to rotate about their centres by virtue of their self-induced velocity. In turn, the self-induced velocity field in the neighbourhood of any given vortex tends to rotate with the vortex. When the velocity due to the rotated and deformed vortices is combined with the vertical component of the strain the result is a net velocity in the vicinity of each vortex which is primarily spanwise and directed toward the centre of the vortex. Figure 5 gives a graphical illustration of this mechanism for the focusing of secondary vortices. If the vortices are strong enough, the focusing effect will not be overcome by viscous diffusion, and collapse will result.

In order to simulate the shear instabilities of highly flattened secondary vortices, the base flow is taken to be a uniform Burgers vortex sheet (Batchelor 1967) with Reynolds number $Re' = \Delta V\delta/\nu$, where ΔV is the total shear. At high Reynolds numbers, the Burgers vortex sheet is unstable to the formation of periodic arrays of rolls, and there arrays are themselves subject to the subharmonic instability that results in the pairwise colescence of rolls. Both rollup and pairing are observed in the numerical simulations.

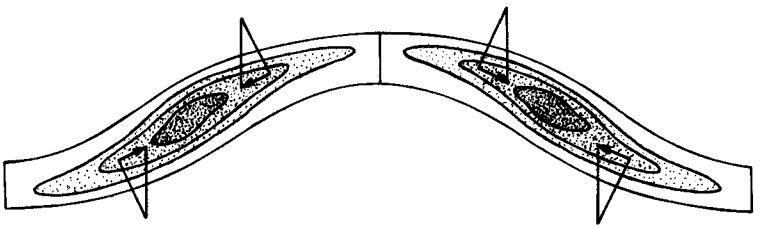

FIGURE 5. The mechanism for collapse of secondary vortices.

3. Vortex-dynamics formulation of the model

We present the governing equations of vortices whose axes are all parallel to the principal axis of a uniform plane strain. Referring to the physical situation depicted in figure 3, we take the vorticity field to be

$$\boldsymbol{\omega} = \omega(x, y, t)\hat{\boldsymbol{z}}, \tag{3.1}$$

and the velocity field of the uniform plane strain to be

$$\boldsymbol{u}_e = -\gamma y\hat{\boldsymbol{y}} + \gamma z\hat{\boldsymbol{z}}. \tag{3.2}$$

The vorticity $\omega(x, y, t)$ satisfies the transport equation

$$\omega_t + (u\omega)_x + ((v-\gamma y)\omega)_y = \nu\Delta\omega, \tag{3.3}$$

where

$$u(x, y, t) = -\frac{1}{2\pi}\int_{-\infty}^{\infty}\int_{-\infty}^{\infty}\frac{(y-y')\,\omega(x', y', t)}{(x-x')^2+(y-y')^2}\,\mathrm{d}x'\,\mathrm{d}y', \tag{3.4}$$

$$v(x, y, t) = \frac{1}{2\pi}\int_{-\infty}^{\infty}\int_{-\infty}^{\infty}\frac{(x-x')\,\omega(x', y', t)}{(x-x')^2+(y-y')^2}\,\mathrm{d}x'\,\mathrm{d}y' \tag{3.5}$$

are the x- and y-components of velocity induced by the vorticity. Equation (3.3) with u and v given by (3.4) and (3.5) constitutes an integro-differential equation for the evolution of the vorticity $\omega(x, y, t)$. The physical content of this evolution equation is that the vorticity is convected by the sum of its self-induced velocity and the inward (y) component of the strain, and diffused by the action of the viscosity.

We present a related formulation that describes stretched vortex sheets in ideal fluid. In this case, the vorticity is given by

$$\omega(x, y, t) = \sigma(x, t)\,\delta(y-\eta(x, t)). \tag{3.6}$$

In (3.6), $\eta(x, t)$ gives the elevation of the vortex sheet and $\sigma(x, t)$ is surface vortex density measured with respect to x: the circulation between x and $x+\mathrm{d}x$ is $\sigma(x, t)\,\mathrm{d}x$. The evolution equations for η and σ are

$$\eta_t + u\eta_x - v + \gamma\eta = 0, \tag{3.7}$$

$$\sigma_t + (u\sigma)_x = 0, \tag{3.8}$$

where u and v are given by the principal-value integrals

$$u = -\frac{1}{2\pi}\int_{-\infty}^{\infty}\frac{\eta-\eta'}{(x-x')^2+(\eta-\eta')^2}\sigma'\,\mathrm{d}x', \tag{3.9}$$

$$v = \frac{1}{2\pi}\int_{-\infty}^{\infty}\frac{x-x'}{(x-x')^2+(\eta-\eta')^2}\sigma'\,\mathrm{d}x'. \tag{3.10}$$

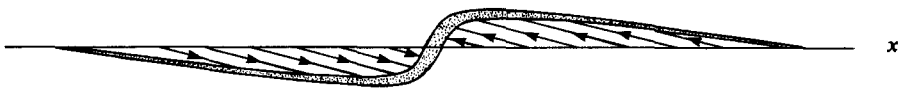

FIGURE 6. Linear instability of a strained vortex sheet.

In (3.9) and (3.10), η' and σ' denote the values of η and σ at $x = x'$. The physical content of (3.7) is that the velocity of a material point at position $x\hat{\boldsymbol{x}}+\eta(x,t)\hat{\boldsymbol{y}}$ on the vortex sheet is the resultant of the y-component of strain, given by $-\gamma y\hat{\boldsymbol{y}}$, and the self-induced velocity, given by $u\hat{\boldsymbol{x}}+v\hat{\boldsymbol{y}}$. The values of u and v given in (3.9) and (3.10) are obtained by substituting the surface δ-function (3.6) for the vorticity into (3.4) and (3.5) and setting $y = \eta(x,t)$. The physical content of (3.8) is that the surface vortex density is a locally conserved quantity.

4. Stretched vortices in ideal fluid

We analyse the collapse of stretched vortices in ideal fluid. We begin with an asymptotic analysis of vortex sheets. A class of similarity solutions to the equations of the asymptotic theory give concrete examples of the vortex-sheet collapse process. These similarity solutions of the asymptotic equations correspond to a new class of exact solutions to the Euler equations. These are discussed in detail. The combined results of asymptotic analysis plus exact solutions give a quantitative description of the Corcos–Lin collapse mechanism discussed in §2.

We inspect the effect of the strain upon the Kelvin–Helmholtz instability of a uniform vortex layer of strength $\sigma = \sigma_0$. From a linearized analysis of the stretched vortex-sheet equations (3.7)–(3.10), we find that there is a mode of temporal instability with

$$\sigma = \mathrm{e}^{\alpha t}\cos kx, \tag{4.1}$$

where the growth rate α is related to the wavenumber k by

$$\frac{\alpha}{\gamma} = \frac{1}{2}\left(1+\frac{\sigma_0^2 k^2}{\gamma^2}\right)^{\frac{1}{2}} - \tfrac{1}{2}. \tag{4.2}$$

For this mode, material points drift away from the x-axis along straight lines with slope

$$m = \frac{\sigma_0 k}{\gamma}\Big/\left(1+\frac{\sigma_0^2 k^2}{\gamma^2}\right)^{\frac{1}{2}}, \tag{4.3}$$

as illustrated in figure 6. In the short-wave limit $\sigma_0 k/\gamma \to \infty$ (4.2) and (4.3) have the asymptotic forms

$$\sigma \sim \tfrac{1}{2}\sigma_0 k, \quad m \sim 1. \tag{4.4}$$

These are the known results for the free vortex sheet without strain. Short-wave disturbances penetrate only a small distance vertically, and so they do not feel the strain. In the long-wave limit $\sigma_0 k/\gamma \to 0$ we have

$$\frac{\alpha}{\gamma} \sim \frac{1}{4}\frac{\sigma_0^2 k^2}{\gamma^2}, \quad m \sim \frac{\sigma_0 k}{\gamma}. \tag{4.5}$$

We see that the strain has a stabilizing effect on long waves in that the dimensionless growth rate α/γ is reduced from $O(\sigma_0 k/\gamma)$ to $O(\sigma_0^2 k^2/\gamma^2)$. Nevertheless, instability is not eliminated entirely, and the fact that $m \sim \sigma_0 k/\gamma$ is small tells why. The compressing effect of the strain kills the vertical drift of vortices, but does not prevent a horizontal drift that serves to focus the strength density.

Variable	σ	η	x	t
Unit	σ^0	$\dfrac{\sigma^0}{\gamma}$	$\dfrac{\sigma^2}{\epsilon\gamma}$	$\dfrac{1}{\epsilon^2\gamma}$

TABLE 1

It is possible to develop a nonlinear theory for the focusing of the strength density in a long-wave limit where the gradient of the strength density σ_x is much less than the strain rate γ. That is

$$\sigma_x \ll \gamma. \tag{4.6}$$

We adopt a non-dimensionalization of the stretched vortex-sheet equations (3.7) and (3.8) with the units of the variables as given in table 1. In table 1 σ^0 is a typical value for the strength density of the initial conditions, and $\epsilon \ll 1$. It is easily seen that the choice of scales in table 1 is consistent with the condition (4.6).

The dimensionless equations are

$$\epsilon^2(\eta_t + U\eta_x) - V + \eta = 0, \tag{4.7}$$

$$\sigma_t = (U\sigma)_x = 0, \tag{4.8}$$

where

$$U \equiv -\frac{1}{2\pi}\int_{-\infty}^{\infty} \frac{\eta-\eta'}{(x-x')^2+\epsilon^2(\eta-\eta')^2}\sigma'\,dx', \tag{4.9}$$

$$V \equiv \frac{1}{2\pi}\int_{-\infty}^{\infty} \frac{x-x'}{(x-x')^2+\epsilon^2(\eta-\eta')^2}\sigma'\,dx'. \tag{4.10}$$

In the limit $\epsilon \to 0$ these reduce to

$$\eta = V, \tag{4.11}$$

$$\sigma_t + (U\sigma)_x = 0, \tag{4.12}$$

where

$$U = -\frac{1}{2\pi}\int_{-\infty}^{\infty} \frac{\eta-\eta'}{(x-x')^2}\sigma'\,dx', \tag{4.13}$$

$$V = \frac{1}{2\pi}\int_{-\infty}^{\infty} \frac{\sigma'}{x-x'}dx'. \tag{4.14}$$

Equation (4.11) says that the vortex layer achieves the elevation η at which the vertical component V of its self-induced velocity balances the strain. It is not a perfectly static equilibrium. From (4.13) we see that the distortion of the vortex layer from the horizontal gives rise to a horizontal component of velocity U, which, according to (4.12), convects the vortices. From (4.14), we see that the change in σ produces a change in V and forces a readjustment of the elevation η.

The system (4.11)–(4.14) can be reduced to a single equation for $\sigma(x,t)$. Combining (4.11), (4.13) and (4.14), we write the horizontal transport velocity U as a functional of σ. The result is

$$U = U[\sigma] \equiv -\frac{1}{4\pi}\int_{-\infty}^{\infty} \frac{\hat{\sigma}-\hat{\sigma}'}{(x-x')^2}\sigma'\,dx', \tag{4.15}$$

where $\hat{f}$ denotes the Hilbert transform of f, given by

$$\hat{f}(x) = \frac{1}{\pi}\int_{-\infty}^{\infty} \frac{f(x')}{x-x'}dx'. \tag{4.16}$$

In the form (4.15), $U[\sigma]$ appears to be a non-local functional of σ, but in fact we have

$$U[\sigma] = \tfrac{1}{4}\sigma\sigma_x \tag{4.17}$$

for any smooth $\sigma(x)$ with a Fourier-series or Fourier-transform representation. The calculation leading from (4.15) to (4.17) is recorded in Appendix A. Here, we simply observe that, with U given by (4.17), the conservation law (4.11) becomes

$$\sigma_t + \tfrac{1}{4}(\sigma^2\sigma_x)_x = 0. \tag{4.18}$$

Equation (4.18) is a backwards heat equation for σ which predicts the focusing of vortex concentrations. The nature of the focusing is easy to see from (4.17). Vortices are convected in the direction of increasing vortex density. There are similarity solutions to (4.18) which represent isolated segments of stretched vortex sheets undergoing collapse. In the original dimensional variables, these solutions are given by

$$\sigma(x,t) = \frac{2\Gamma}{\pi a(t)}\left(1 - \frac{x^2}{a^2(t)}\right)^{\frac{1}{2}} \tag{4.19}$$

in $|x| < a(t)$, and $\sigma(x,t) \equiv 0$ in $|x| > a(t)$, where

$$a(t) \equiv a_0\left(1 - \frac{4\Gamma^2}{\pi^2\gamma^2 a_0^4}\gamma t\right)^{\frac{1}{4}}. \tag{4.20}$$

In these formulas, Γ is the total circulation of the segment, a_0 is its initial half-length at time $t = 0$, and $a(t)$ is its half-length at time t. We see from (4.20) that the segment collapses to a point vortex in time t_c given by

$$\gamma t_c = \frac{\pi^2\gamma^2 a_0^4}{4\Gamma^2}. \tag{4.21}$$

From (4.11) and (4.14) we find that the interfacial elevation corresponding to the elliptical strength density profile (4.19) is a linear function of x, given by

$$\eta(x,t) = \frac{\Gamma x}{\pi\gamma a^2(t)}. \tag{4.22}$$

Figures 7 (a, b) are sequences of snapshots depicting the evolutions of σ and η as given by the similarity solution. The condition for the validity of the asymptotic theory is that $\sigma_x \ll \gamma$. Applying this criterion to the similarity solutions, we find that it is valid only when $\Gamma/\gamma a^2(t) \ll 1$. We see from (4.22) that this implies small values for the slope of the vortex sheet with respect to the horizontal.

There are exact solutions of the Euler equations directly related to the similarity solutions of the asymptotic equation (4.18). These exact solutions correspond to uniform elliptical vortices undergoing rotation, deformation and compression in a uniform plane strain which is parallel to the vortex axis. Figure 8 shows the physical situation we are considering. The elliptical cylinder of uniform vorticity is centred about the z-axis. The inward y component of the strain is $-\gamma y\hat{\mathbf{y}}$. The major and minor axes of the ellipse are denoted by a and b. The angle of orientation of the major axis with respect to the x-axis is θ. a, b and θ are time-dependent quantities that evolve according to the equations

$$\dot{a} = -(\gamma \sin^2\theta)\, a, \tag{4.23}$$

$$\dot{b} = -(\gamma \cos^2\theta)\, b, \tag{4.24}$$

$$\dot{\theta} = \frac{\Gamma}{\pi(a+b)^2} - \frac{\gamma}{2}\frac{a^2+b^2}{a^2-b^2}\sin 2\theta, \tag{4.25}$$

where Γ is the total circulation around the ellipse.

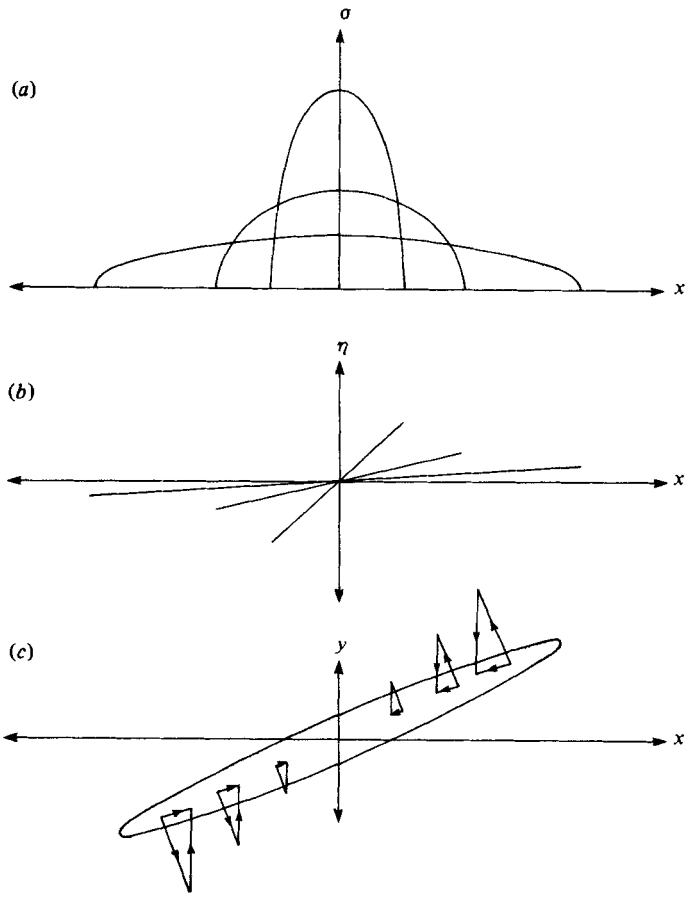

FIGURE 7. Vortex-sheet collapse according to the inviscid theory.

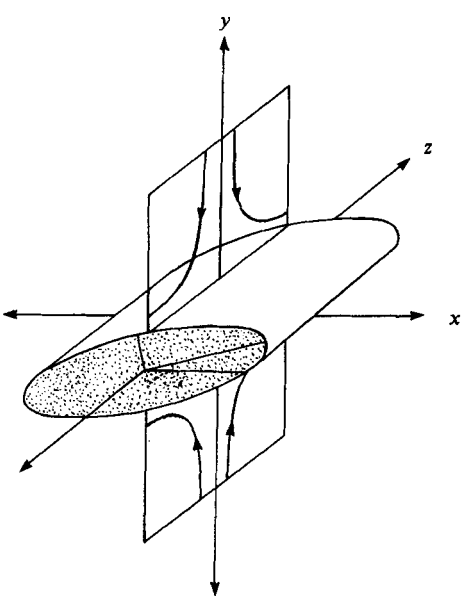

FIGURE 8. A strained elliptical vortex.

The existence of such solutions is based on the fact that the component

$$\boldsymbol{u}_{\mathrm{p}} = u_{\mathrm{p}}\hat{\boldsymbol{x}} + v_{\mathrm{p}}\hat{\boldsymbol{y}}$$

of velocity in the (x, y)-plane due to the combined influences of the vortex and the strain is a linear function of $\boldsymbol{x} = x\hat{\boldsymbol{x}} + y\hat{\boldsymbol{y}}$ inside the ellipse. $\boldsymbol{u}_{\mathrm{p}}$ is given by

$$\boldsymbol{u}_{\mathrm{p}} = \boldsymbol{U}(a, b, \theta)\,\boldsymbol{x}, \tag{4.26}$$

where the matrix

$$\boldsymbol{U}(a, b, \theta) \equiv -\frac{\Gamma}{\pi ab(a+b)}\boldsymbol{R}(\theta)\begin{pmatrix} 0 & a \\ -b & 0 \end{pmatrix}\boldsymbol{R}(\theta) - \gamma\begin{pmatrix} 0 & 0 \\ 0 & 1 \end{pmatrix}. \tag{4.27}$$

In (4.27), the standard rotation matrix

$$\boldsymbol{R}(\theta) \equiv \begin{pmatrix} \cos\theta & -\sin\theta \\ \sin\theta & \cos\theta \end{pmatrix}. \tag{4.28}$$

The result (4.26) is obtained from a single potential-theory calculation outlined in Lamb (1932). The first term of the matrix (4.27) represents the velocity induced by the vortex. The self-induced velocity inside a rotated ellipse may be obtained by rotating the velocity field inside of the $\theta = 0$ ellipse. This accounts for the presence of rotation matrices $\boldsymbol{R}(\theta)$ and $\boldsymbol{R}(-\theta)$. The second term in (4.27) represents the strain. The consequence of (4.26) is that material lines inside the vortex that are parallel to the z-axis are mapped from their initial positions to subsequent positions at a later time by a linear transformation. It follows that a uniform elliptical vortex will remain uniform and elliptical for all time. The evolution of the vortex is fully specified if the ellipse parameters a, b, θ are determined as functions of time. Starting from the formula (4.26) for the component $\boldsymbol{u}_{\mathrm{p}}$ of velocity in the (x, y)-plane, one can straightforwardly deduce the equations (4.23)–(4.25) for a, b and θ.

The special case of (4.23)–(4.25) relevant to vortex sheets is $b = 0$. In this case, the elliptical vortex degenerates into a flat vortex sheet with strength density profile

$$\sigma = \frac{2\Gamma}{\pi a}\left(1 - \frac{s^2}{a^2}\right)^{\frac{1}{2}}, \tag{4.29}$$

where s is distance from the centre of the sheet. The half-length a of the sheet and its orientation angle θ satisfy the equations

$$\dot{a} = -(\gamma \sin^2\theta)\,a, \tag{4.30}$$

$$\dot{\theta} = \frac{\Gamma}{\pi a^2} - \frac{\gamma}{2}\sin 2\theta. \tag{4.31}$$

The asymptotic theory treats the collapse of sheets with $\epsilon \equiv \Gamma/\gamma a_0^2 \ll 1$. To recover the results of the asymptotic theory from the exact equations (4.30) and (4.31), we measure a in units of $\Gamma/\epsilon\gamma a_0$, θ in units of ϵ, and time in units of $1/\epsilon^2\gamma$. The dimensionless equations are

$$\epsilon^2\dot{a} = -(\sin^2\epsilon\theta)\,a, \tag{4.32}$$

$$\epsilon^2\dot{\theta} = \frac{1}{\pi a^2} - \frac{1}{\epsilon}\cos\epsilon\theta\sin\epsilon\theta. \tag{4.33}$$

In the limit $\epsilon \to 0$ these equations become

$$\dot{a} = -\theta^2 a, \quad \theta = \frac{1}{\pi a^2}. \tag{4.34}$$

The solution with $a(0) = 1$ is

$$a = \left(1 - \frac{t}{\pi^2}\right)^{\frac{1}{4}}, \tag{4.35}$$

which we recognize as the dimensionless version of (4.20).

Figure 7(*c*) illustrates the physics responsible for the collapse of a lightly elongated elliptical vortex. The arrows perpendicular to the major axis represent the vortex-induced velocity along the major axis. The vertical arrows represent the component of strain in the (x, y)-plane. We see that the sum of vortex- and strain-induced velocities is primarily spanwise and directed toward the centre of the vortex, causing it to collapse in the manner described by Corcos and Lin.

5. Stretched vortices in viscous fluid

The viscous vorticity equation (3.3) has a solution

$$\omega = \sigma\left(\frac{\gamma}{2\pi\nu}\right)^{\frac{1}{2}} \exp\left(-\frac{\gamma}{2\nu}y^2\right), \tag{5.1}$$

which represents a vortex layer with thickness $\delta = (\pi\nu/2\gamma)^{\frac{1}{2}}$ and circulation σ per unit distance in the spanwise (x) direction. This solution is the well-known Burgers vortex sheet. The thickness δ is determined by a balance between the strain, which tends to compress the vortex layer, and the viscous diffusion, which tends to disperse it.

If the circulation per unit spanwise length

$$\sigma(x,t) \equiv \int_{-\infty}^{\infty} \omega(x,y,t)\,\mathrm{d}y \tag{5.2}$$

is slowly varying in the sense that $\sigma_x \ll \gamma$, the vorticity distribution remains nearly Gaussian in the y direction, but its centre of mass

$$\eta(x,t) \equiv \frac{1}{\sigma(x,t)}\int_{-\infty}^{\infty} y\omega(x,y,t)\,\mathrm{d}y \tag{5.3}$$

deflects from the x-axis. Accordingly, the vorticity field is given to leading order by

$$\omega(x,y,t) \sim \sigma(x,t)\left(\frac{\gamma}{2\pi\nu}\right)^{\frac{1}{2}} \exp\left[-\frac{1}{2}\frac{\gamma}{\nu}(y-\eta(x,t))^2\right]. \tag{5.4}$$

The dynamics of the vortex layer is determined by the evolution of $\sigma(x,t)$ and $\eta(x,t)$.

We begin by proposing heuristic equations for ν and η based upon our knowledge of the inviscid case. These equations are

$$\sigma_t + \left(\left(\frac{1}{4\gamma}\sigma^2 - \nu\right)\sigma_x\right)_x = 0, \tag{5.5}$$

$$\gamma\eta = \frac{1}{2\pi}\int_{-\infty}^{\infty} \frac{\sigma'}{x-x'}\,\mathrm{d}x' = \tfrac{1}{2}\hat{\sigma}. \tag{5.6}$$

Equation (5.5) is the viscous analogue of the inviscid transport equation (4.18). Equation (5.5) says that σ is a locally conserved quantity whose flux is

$$F = \left(\frac{1}{4\gamma}\sigma\sigma_x\right)\sigma - \nu\sigma_x. \tag{5.7}$$

The first term in (5.7) represents the flux due to transport of vortices by bulk fluid motion, as in (4.18). The second term is the flux due to viscous diffusion. Equation

(5.6) states that the centreline of the vortex layer seeks the elevation at which the vertical components of the vortex- and strain-induced velocities balance. This remains the same as in the inviscid theory.

We will show in §6 that (5.5) and (5.6) are in fact the leading-order equations for σ and η when $\sigma_x \ll \gamma$ and $\sigma^2/\nu\gamma = O(1)$. The first of these conditions corresponds to the long-wave limit evoked in the inviscid theory. The second condition corresponds to a balance between the fluxes of vorticity due to bulk fluid motion and viscous diffusion. In the remainder of this section we investigate the collapse of secondary vortices as described by (5.5) and (5.6).

Equation (5.5) may be viewed as a nonlinear diffusion equation with diffusivity

$$D(\sigma) \equiv \nu - \frac{1}{4\gamma}\sigma^2. \tag{5.8}$$

If

$$|\sigma| > 2(\nu\gamma)^{\frac{1}{2}}, \tag{5.9}$$

the diffusivity is negative and we expect that intervals of a vortex layer where this condition is satisfied will collapse to produce concentrated vortices.

The mechanics of the collapse process may be understood by studying the evolution of $\sigma(x,t)$ from specific initial conditions. First we consider the evolution of $\sigma(x,t)$ from an initial condition $\sigma = \sigma(x,0)$ with $|\sigma(x,0)| < 2(\nu\gamma)^{\frac{1}{2}}$ inside of an interval $X_- < x < X_+$ and $|\sigma(x,0)| \equiv 2(\nu\gamma)^{\frac{1}{2}}$ outside. For such initial conditions, we have $D(\sigma) > 0$ in the interior of $X_- < x < X_+$ and $D(\sigma) \equiv 0$ in the exterior. We require $\sigma(x,0)$ to be continuous at $x = X_\pm$ and the derivative $\sigma_x(x,0)$ to have finite non-zero left- and right-hand limits at $x = X_-$ and $x = X_+$. A typical example of such an initial condition is depicted by the thin curve in figure 9(*a*). Using some basic facts about initial-value problems for nonlinear heat equations, we can describe certain features of the subsequent evolution. At any $t > 0$ for which the solution exists, there is an interval $x_-(t) < x < x_+(t)$ so that $|\sigma(x,t)| < 2(\nu\gamma)^{\frac{1}{2}}$ inside this interval and $|\sigma(x,t)| \equiv 2(\nu\gamma)^{\frac{1}{2}}$ outside this interval. The endpoints $x_-(t)$ and $x_+(t)$ move to the left and right at speeds proportional to the derivatives $\sigma_x(x_-^+(t),t)$ and $\sigma_x(x_+^-(t),t)$. Since we expect diffusion to diminish the gradient σ_x, the expansion of the interval $x_-(t) < x < x_+(t)$ slows down with time. The thicker curve in figure 9(*b*) represents the solution at time $t > 0$ which evolved from the initial condition at $t = 0$ represented by the thinner curve.

We now consider the evolution of $\sigma(x,t)$ from an initial condition which differs from the previous case in that $|\sigma(x,0)| > 2(\nu\gamma)^{\frac{1}{2}}$ inside $X_- < x < X_+$. The diffusivity $D(\sigma)$ is negative in $X_- < x < X_+$. The initial-value problem consisting of (5.5) subject to such an initial condition is ill-posed. Nevertheless, we can construct special solutions with $|\sigma(x,t)| > 2(\nu\gamma)^{\frac{1}{2}}$ which represent vortex-sheet collapse. These are obtained from time reversals of solutions to the time-reversed equations $\sigma_t = -(D(\sigma)\sigma_x)_x$ subject to the same class of initial data. The time-reversed equation represents forward diffusion, so it evolves highly concentrated initial distributions of σ into more-diffuse distributions. The time reversals of such evolutions give the required examples of collapse. The circulation excess Γ_c inside the collapsing interval $x_-(t) < x < x_+(t)$ where $|\sigma| > 2(\nu\gamma)^{\frac{1}{2}}$ is defined by

$$\Gamma_c = \int_{x_-(t)}^{x_+(t)} (\sigma(x,t) - 2(\nu\gamma)^{\frac{1}{2}})\, dx. \tag{5.10}$$

This is a conserved quantity. A consequence is that the collapsing distribution must steepen as the interval $x_-(t) < x < x_+(t)$ shrinks, so that the values of the gradient σ_x at $x = x_-^+(t)$ and $x = x_+^-(t)$ are expected to increase with time. As a result, the

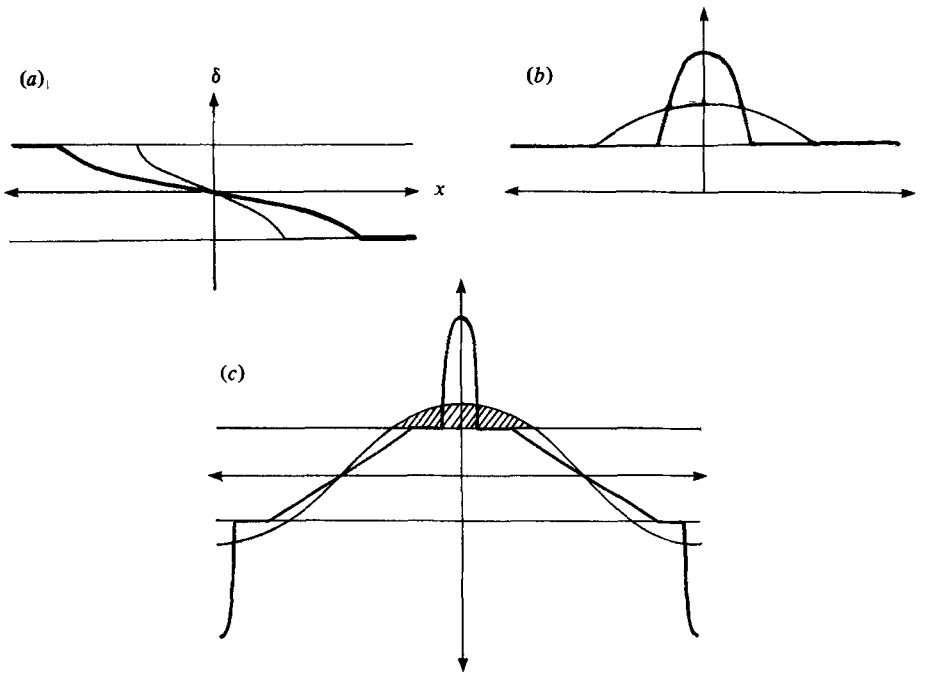

FIGURE 9. Evolutions of a strained vortex sheet in ideal fluid.

collapse accelerates with time. A collapse of a vortex sheet into a concentrated vortex, if that indeed happens, takes place in a finite time. Figure 9(*b*) depicts an example of such a collapse process. The thinner curve represents the initial distribution and the thicker curve the collapsed distribution at a later time.

On the basis of the special solutions discussed so far, we present a conjecture of how a periodic array of alternating vortices with wavelength λ and circulation Γ per vortex undergoes collapse. The lightened curve in figure 9(*c*) represents the initial condition

$$\sigma(x,0) = \frac{\pi\Gamma}{\lambda}\sin\frac{2\pi}{\lambda}x, \tag{5.11}$$

which gives a specific example of such an array. There are regions where $|\sigma| > 2(\nu\gamma)^{\frac{1}{2}}$ if

$$\frac{\Gamma}{\lambda} > \frac{2}{\pi}(\nu\gamma)^{\frac{1}{2}}. \tag{5.12}$$

An alternative form of (5.12) is

$$\Gamma^* a > \frac{1}{8}\left(\frac{2}{\pi}\right)^{\frac{3}{2}} \approx 0.064, \tag{5.13}$$

where $\Gamma^* \equiv \Gamma/8\gamma\lambda^2$ is the non-dimensional circulation and $a \equiv \lambda/\gamma$ is the aspect ratio.

Equation (5.12) is a criterion for collapse in an array with

$$\sigma_x = O\left(\frac{\gamma}{\lambda^2}\right) \ll \gamma. \tag{5.14}$$

We assume that the parameters λ, Γ, ν and γ satisfy (5.12) and (5.13).

The thick curve in figure 9(*c*) shows the conjectured solution for $\sigma(x,t)$ at a time $t > 0$. The intervals where $|\sigma| < 2(\nu\gamma)^{\frac{1}{2}}$ grow, but we expect this growth is slower than

Variable	ω	u	v	x	y	t
Units	$\sigma^0\left(\frac{\gamma}{\nu}\right)^{\frac{1}{2}}$	σ^0	σ^0	$\frac{\sigma^0}{\epsilon\gamma}$	$\left(\frac{\nu}{\gamma}\right)^{\frac{1}{2}}$	$\frac{1}{\epsilon^2\gamma}$

TABLE 2

the collapse of regions where $|\sigma| > 2(\nu\gamma)^{\frac{1}{2}}$. As a result, the collapse process results in concentrated vortices surrounded by plateaus where σ has uniform value $+2(\nu\gamma)^{\frac{1}{2}}$ or $-2(\psi\gamma)^{\frac{1}{2}}$. The collapsed vortices have strength Γ_c equal to the circulation excess of the initial distribution. This circulation excess is numerically equal to the area of the hatched region in figure 9(*c*). In between two plateaus of opposite sign, σ changes continuously from $-2(\nu\gamma)^{\frac{1}{2}}$ to $+2(\nu\gamma)^{\frac{1}{2}}$ in a region which corresponds to interdiffusion of positive and negative strength density. The growth of these regions means that the plateaus are eventually consumed by the interdiffusion process.

6. The symptotic theory

The nonlinear diffusion equation (5.5) that governs the vortex-layer strength $\sigma(x,t)$ to leading order is ill-posed for initial conditions $\sigma(x,0)$ whose maximum absolute value exceeds $2(\nu\gamma)^{\frac{1}{2}}$. Solutions evolved from such initial data develop singularities in finite time. In regions where $|\sigma(x,t)| > 2(\nu\gamma)^{\frac{1}{2}}$, the negative diffusivity $D(\sigma) = \nu - \sigma^2/4\gamma$ causes perturbations in σ with the smallest spatial scales grow the fastest. None of these pathological behaviours are expected for real flows in viscous fluid. We resolve these difficulties by a careful asymptotic analysis of the full viscous vorticity equations (3.3) which yields the nonlinear diffusion equation (5.5) at leading order, together with higher-order corrections which act to stabilize fluctuations in σ with small spatial scales. To single out the asymptotic limit $\sigma_x \ll \gamma$, $\sigma^2/\nu\gamma = O(1)$, we adopt a non-dimensionalization of the viscous vorticity equation (3.3) with the units of the variables as given in table 2. In table $2\sigma^0$ is a typical value of the circulation per unit length of the initial conditions and $\epsilon \ll 1$. The units of x and t are the same as in the inviscid theory of §4. The unit of y is essentially the thickness of the Burgers vortex sheet. A vortex layer with circulation σ^0 per unit length generates velocities of the same order. That is why u and v are measured in units of σ^0. The unit of vorticity is the shear σ^0 divided by the vortex-layer thickness.

The dimensionless vorticity equation is

$$\omega_{yy} + \left(\left(y - \frac{v}{\mu}\right)\omega\right)_y = \epsilon(u\omega)_x + \epsilon^2(\omega_t - \mu^2\omega_{xx}), \tag{6.1}$$

where

$$u = -\frac{\epsilon\mu}{2\pi}\int_{-\infty}^{\infty}\int_{-\infty}^{\infty}\frac{(y-y')\,\omega(x',y',t)}{(x-x')^2+\epsilon^2\mu^2(y-y')^2}\,dx'\,dy', \tag{6.2}$$

$$v = \frac{1}{2\pi}\int_{-\infty}^{\infty}\int_{-\infty}^{\infty}\frac{(x-x')\,\omega(x',y',t)}{(x-x')^2+\epsilon^2\mu^2(y-y')^2}\,dx'\,dy'. \tag{6.3}$$

In (6.1)–(6.3) $\mu^2 \equiv \nu\gamma/\sigma^{02}$ is the non-dimensional viscosity. In this analysis μ is assumed to be $O(1)$.

We present the asymptotic analysis of (6.1)–(6.3). We consider solutions of the

vorticity equation which represent shear layers whose circulation per unit spanwise length

$$\sigma(x,t) = \int_{-\infty}^{\infty} \omega(x,y,t)\,\mathrm{d}y \tag{6.4}$$

is finite. The object of this analysis is to determine the equation of evolution for $\sigma(x,t)$.

This is the strategy of the analysis: We attempt to construct an asymptotic solution

$$\omega \sim \omega^0 + \epsilon\omega^1 + \epsilon^2\omega^2 + \ldots \tag{6.5}$$

of the vorticity equation (6.1) with a prescribed value of $\sigma(x,t)$. This of course cannot be done for arbitrary $\sigma(x,t)$, but only for those $\sigma(x,t)$ which obey a certain evolution equation

$$\sigma_t = (f(\epsilon))\,[\sigma] = f^0[\sigma] + \epsilon f^1[\sigma] + \epsilon^2 f^2[\sigma] + \ldots. \tag{6.6}$$

The functionals $f^j[\sigma]$ are determined from the solvability conditions of the perturbation equations for the ω^j. We see that carrying out the analysis to higher order extends the asymptotic solution's domain of validity in time.

The first step in implementing the above strategy is to obtain asymptotic expansions of the integrals (6.2) and (6.3) for u and v in the limit $\epsilon \to 0$. Straightforward expansions of the integrands in powers of ϵ lead to divergent integrals. The crucial idea is to apply contour integration to the x' variable. The final results of the asymptotic evaluations are

$$u \sim -\frac{1}{2}\int_{-\infty}^{\infty} \{\operatorname{sgn}(y-y')\,\omega' + \epsilon\mu(y-y')\,\hat{\omega}'_x - \tfrac{1}{2}\epsilon^2\mu^2 \operatorname{sgn}(y-y')\,(y-y')^2\,\omega'_{xx} + \ldots\}\,\mathrm{d}y', \tag{6.7}$$

$$v \sim \frac{1}{2}\int_{-\infty}^{\infty} \{\hat{\omega}' + \epsilon\mu\,|y-y'|\,\omega'_x - \tfrac{1}{2}\epsilon^2\mu^2\,(y-y^2)\,\hat{\omega}'_{xx} + \ldots\}\,\mathrm{d}y'. \tag{6.8}$$

Here ω' denotes $\omega(x,y',t)$, and $\hat{f}(x)$ denotes the Hilbert transform of $f(x)$ given by (4.15). The calculations leading to (6.7) and (6.8) are recorded in Appendix B.

From (6.1), and (6.8), we can determine the perturbation equations for the ω^j. The equation for ω^0 is

$$\omega^0_{yy} + \left(\left(y - \frac{v^0}{\mu}\right)\omega^0\right)_y = 0, \tag{6.9}$$

where

$$v^0 = \frac{1}{2}\int_{-\infty}^{\infty} \hat{\omega}^{0\prime}\,\mathrm{d}y'. \tag{6.10}$$

From (6.10), we see that v^0 is independent of y. Hence the unique solution of (6.10) for ω^0 with $\int_{-\infty}^{\infty} \omega^{0\prime}\,\mathrm{d}y' = \sigma$ is

$$\omega^0 = \frac{\sigma}{(2\pi)^{\frac{1}{2}}} \exp\left[-\frac{1}{2}\left(y - \frac{v^0}{\mu}\right)^2\right]. \tag{6.11}$$

With this solution for ω^0, we find from (6.10) that

$$v^0 = \tfrac{1}{2}\hat{\sigma}. \tag{6.12}$$

We recognize (6.11) and (6.12) as the dimensionless forms of (5.4) and (5.6) which describe a Burgers vortex sheet whose centreline deflects from the x-axis owing to the inhomogeneities in $\sigma(x,t)$.

Given the leading-order solution for ω^0 in terms of σ, we attempt to solve the higher-order equations for ω^j, $j \geqslant 1$. Since $\int_{-\infty}^{\infty} \omega^0\,\mathrm{d}y = \sigma$, we seek solutions for ω^j,

$j \geqslant 1$, with $\int_{-\infty}^{\infty} \omega^j \, dy = 0$ in order to have $\int_{-\infty}^{\infty} \omega \, dy = \sigma$ overall. This can be achieved only if certain solvability conditions are satisfied. The solvability conditions are determined as follows:

By integrating equations (6.1) with respect to y from $-\infty$ to $+\infty$, we find

$$\sigma_t + (F - \mu^2 \sigma_x)_x = 0, \tag{6.13}$$

where

$$F \equiv \frac{1}{\epsilon} \int_{-\infty}^{\infty} u\omega \, dy \tag{6.14}$$

is the net flux of vorticity in the spanwise direction due to the spanwise velocity u. Inserting into (6.14) the asymptotic expansion for u given in (6.7), we find a convenient asymptotic expansion for F:

$$F \sim \tfrac{1}{2}\mu \int_{-\infty}^{\infty} \int_{-\infty}^{\infty} (y - y') \hat{\omega}_x' \omega \, dy' \, dy + \tfrac{1}{4}\epsilon\mu^2 \int_{-\infty}^{\infty} \int_{-\infty}^{\infty} \operatorname{sgn}(y - y') (y - y')^2 \omega_{xx}' \omega \, dy' \, dy + \ldots. \tag{6.15}$$

Comparing (6.6) and (6.13), we see that the functional $(f(\epsilon))[\sigma]$ must satisfy

$$(f(\epsilon))[\sigma] + (F - \mu^2 \sigma_x)_x = 0. \tag{6.16}$$

Equations for the $f^j[\sigma]$ are obtained by expanding (6.16) in powers of ϵ. From (6.16) and (6.18), we find that the equation for $f^0[\sigma]$ is

$$\left.\begin{aligned} &f^0[\sigma] + (F^0 - \mu^2 \sigma_x)_x = 0, \\ &F^0 \equiv \tfrac{1}{2}\mu \int_{-\infty}^{\infty} \int_{-\infty}^{\infty} (y - y') \hat{\omega}_x^{0\prime} \omega^0 \, dy' \, dy. \end{aligned}\right\} \tag{6.17}$$

Equation (6.17) turns out to be the solvability condition of the perturbation equation for ω^2. In general, the equation for $f^n[\sigma]$ is the solvability condition of the perturbation equation for ω^{n+2}.

Since ω^0 is known in terms of σ through (6.11), F^0 can be computed explicitly as a functional of σ. We find

$$F^0 = \tfrac{1}{4}\sigma^2 \sigma_x. \tag{6.18}$$

The details of the calculation are recorded in appendix C. With this result for F^0, we find that $f^0[\sigma]$ has the value

$$f^0[\sigma] = ((\mu^2 - \tfrac{1}{4}\sigma^2)\sigma_x)_x. \tag{6.19}$$

The values of the $f^n[\sigma]$ for $n \geqslant 1$ can be found by carrying out the perturbation procedure outlined above to higher order. The result for $f^1[\sigma]$ is

$$f^1[\sigma] = \frac{\mu}{2(2\pi)^{\frac{1}{2}}} ((\sigma^2 \hat{\sigma}_x)_x + c(\sigma(\sigma\sigma_x)_x - \sigma\sigma_x \hat{\sigma}_x))_x, \tag{6.20}$$

where

$$c = 1 + \tfrac{1}{2}(\tfrac{1}{2}\pi)^{\frac{1}{2}} \int_{-\infty}^{\infty} (1 - \operatorname{erf}^2(\sqrt{\tfrac{1}{2}}y)) \, dy \approx 2.2. \tag{6.21}$$

We can now state the main result of the analysis: with $f^0[\sigma]$ and $f^1[\sigma]$ given by (6.19) and (6.20), the evolution equation for $\sigma(x, t)$ reads

$$\sigma_t = ((\mu^2 - \tfrac{1}{4}\sigma^2)\sigma_x)_x + \frac{\epsilon\mu}{2(2\pi)^{\frac{1}{2}}} ((\sigma^2 \hat{\sigma}_x)_x + c(\sigma(\sigma\sigma_x)_x - \sigma\sigma_x \hat{\sigma}_x))_x + \ldots. \tag{6.22}$$

When $\epsilon = 0$, (6.22) reduces to the dimensionless version of the nonlinear diffusion equation (5.5). In §7 we show that the $O(\epsilon)$ correction term stabilizes perturbations in σ with small spatial scales.

7. Kelvin–Helmholtz waves in the Burgers vortex sheet

We apply the evolution equation (6.22) to study Kelvin–Helmholtz waves in a Burgers vortex sheet. We discuss the linearized stability of the uniform Burgers vortex sheet with circulation σ_0 per unit length. The uniform steady solution of the dimensionless equation (6.22) corresponding to this vortex sheet is $\sigma \equiv 1$. The linearized equation for $s \equiv \sigma - 1$ is

$$s_t = (\mu^2 - \tfrac{1}{4})\, s_{xx} + \epsilon\mu\kappa \hat{s}_{xxx} + O(\epsilon^2), \tag{7.1}$$

where $\kappa \equiv (1+c)/2(2\pi)^{\frac{1}{2}} \approx 0.64$. Equation (7.1) possesses spatially periodic solutions

$$s = \mathrm{e}^{\alpha t} \cos kx, \tag{7.2}$$

where the growth rate α is related to the wavenumber k by the dispersion relation

$$\alpha = (\tfrac{1}{4} - \mu^2)\, k^2 - \epsilon\kappa\mu |k|^3 + O(\epsilon^2). \tag{7.3}$$

There are unstable modes with $\alpha > 0$ if and only if

$$\mu < \tfrac{1}{2}. \tag{7.4}$$

Setting μ to its value $(\nu\gamma)^{\frac{1}{2}}/\sigma_0$, we see that (7.4) is identical with the criterion for instability (5.9) obtained in the leading-order theory. The instability criterion (7.4) may also be expressed in terms of the Reynolds number $Re' = \sigma_0 \delta/\nu$ which characterizes the Burgers vortex sheet. We find that (7.4) is equivalent to

$$Re' > (2\pi)^{\frac{1}{2}} \approx 2.51. \tag{7.5}$$

If $\mu < \frac{1}{2}$ and $\epsilon = 0$, we see from (7.3) that the growth rate α diverges to $+\infty$ as $|k| \to \infty$. This is the previously noted failing of the leading-order theory. If $\mu < \frac{1}{2}$ and $\epsilon \neq 0$, there is only a finite band of unstable wavenumbers. To study this case, we take

$$\mu = \tfrac{1}{2} - \tfrac{1}{2}\epsilon\kappa m, \tag{7.6}$$

where $m > 0$ is $O(1)$. In this limit, the first two terms on the right-hand side of (7.3) are both $O(\epsilon)$ and balance each other, but dominate the $O(\epsilon^2)$ correction. We have

$$\alpha = \tfrac{1}{2}\epsilon\kappa(mk^2 - |k|^3) + O(\epsilon^2). \tag{7.7}$$

Figure 10 shows graphs of the dispersion relation (7.7) for various values of m. In the case $m > 0$ the band of unstable wavenumbers is

$$|k| < m + O(\epsilon). \tag{7.8}$$

The wavenumber of maximum instability is

$$k_{\mathrm{M}} = \tfrac{2}{3}m + O(\epsilon). \tag{7.9}$$

To study finite-amplitude Kelvin–Helmholtz waves we take

$$\sigma(x,t) = 1 + \epsilon\kappa s(x,t). \tag{7.10}$$

Substituting (7.10) into the evolution equation (6.22) for $\sigma(x,t)$, we find the equation for $s(x,t)$ to be

$$s_t = -\tfrac{1}{2}\epsilon\kappa((m+s)\, s_x - \hat{s}_{xx})_x + O(\epsilon^2). \tag{7.11}$$

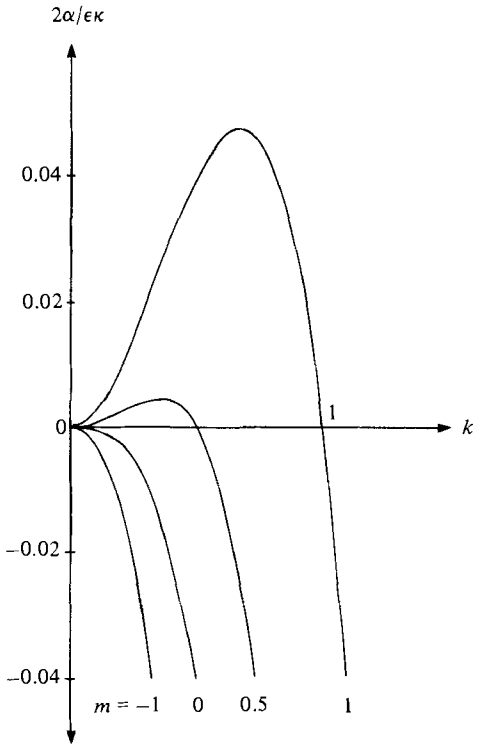

FIGURE 10. Dispersion relations for Kelvin–Helmholtz waves in the Burgers vortex sheet.

In (7.11) the nonlinear term $(ss_x)_x$ balances the linear term $(ms_x - \hat{s}_{xx})_x$ in magnitude. This is the idea behind the scaling (7.10).

Time-independent solutions of (7.11) that are bounded as $|x| \to \infty$ satisfy

$$\hat{s}_{xx} = (m+s)\, s_x. \tag{7.12}$$

Equation (7.12) arises in other contexts, such as the theory of deep internal waves (Benjamin 1967). Certain exact solutions are known. One solution is

$$s(x) = -\frac{4m}{1+m^2x^2}, \tag{7.13}$$

valid for $m < 0$. The corresponding solution for $\sigma(x)$ is

$$\sigma(x) = 1 + 4(2\mu - 1) \Big/ \left(1 + \left(\frac{2\mu-1}{\kappa\epsilon} x^2\right)^2\right) + \ldots, \tag{7.14}$$

valid for $0 < \mu - \frac{1}{2} = O(\epsilon)$. Equation (7.14) represents an isolated vortex concentration in an otherwise uniform shear layer. Figure 11 depicts qualitatively the vorticity contours in the (x, y)-plane corresponding to this vortex concentration. The self-induced velocity of the vortex rotates it slightly from the horizontal. The surrounding uniform shear layer is linearly stable on account of the condition $\mu > \frac{1}{2}$.

Equation (7.12) also possesses periodic solutions with zero mean value. These are given by

$$s(x) = \frac{2k^2}{2k - m - ((2k-m)^2 - k^2)^{\frac{1}{2}} \cos kx} - 2k, \tag{7.15}$$

FIGURE 11. An isolated vortex concentration in the Burgers vortex sheet.

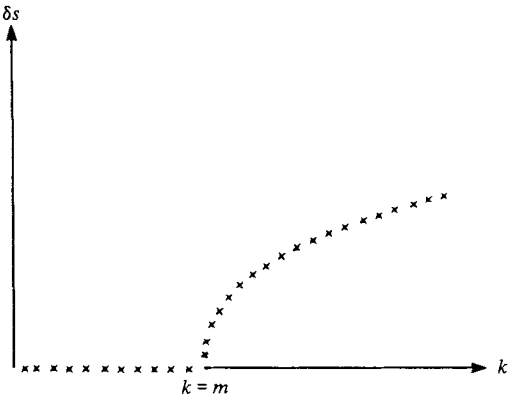

FIGURE 12. Bifurcation diagram.

where $k > \max(m, 0)$. Equation (7.15) represents an array of vortex concentrations with wavenumber k. The solution (7.13) for an isolated vortex concentration is recovered from (7.15) in the limit $k \to 0$. The variation of $s(x)$ over one period is given by

$$\delta s \equiv \max s(x) - \min s(x) = 4((2k-m)^2 - k^2)^{\frac{1}{2}}. \tag{7.16}$$

The parabola in figure 12 depicts δs as a function of k for fixed $m > 0$. We regard figure 12 as a bifurcation diagram. The branch of steady periodic solutions (7.15) bifurcates from the zero-solution at $m = k$. From the linearized stability theory we recall that the zero-solution is unstable for $0 < k < m$ and stable for $k > m$. This means that the bifurcation at $k = m$ is subcritical, with the branch of steady periodic solutions unstable in some interval of k-values whose lower bound is m. In figure 12, stable solution branches are indicated by solid curves and unstable branches by hatched curves.

We can actually show that the steady periodic solutions (7.15) are unstable for all $k > \max(m, 0)$. The stability analysis is based on the fact that the equation (7.11) for $s(x, t)$ has the Lypanov function

$$F[s] \equiv \frac{k}{2\pi} \int_0^{2\pi/k} (\tfrac{1}{2}ms^2 + \tfrac{1}{6}s^2 + \tfrac{1}{2}\hat{s}s_x)\, dx. \tag{7.17}$$

In (7.17) s is $2\pi/k$-periodic in x. For any $2\pi/k$-periodic solution of (7.11), $F[s]$ is non-increasing with rate of change

$$\dot{F} = -\frac{k}{2\pi} \int_0^{2\pi/k} ((m+s)\, s_x - \hat{s}_{xx})^2\, dx. \tag{7.18}$$

A steady solution $s = s_0(x)$ is stable if it is an isolated minimum of F with respect to variations $\delta s(x)$ with zero mean value. It is sufficient to consider variations with zero mean because (7.11) is a conservation law. If in any neighbourhood of $s_0(x)$ there

ω	$\boldsymbol{u}$	x	t
$\Gamma\frac{\gamma}{\nu}$	$\Gamma\left(\frac{\gamma}{\nu}\right)^{\frac{1}{2}}$	$\left(\frac{\psi}{\gamma}\right)^{\frac{1}{2}}$	$\frac{1}{\gamma}$

TABLE 3

is a test function $\phi(x)$ with the same mean as $s_0(x)$ with $F[\phi] < F[s_0]$, then $s_0(x)$ is an unstable steady solution.

To establish the instability of the periodic steady solutions (7.18), we consider the family of test functions

$$\phi(x;h) \equiv 2k\left(\frac{1}{h-(h^2-1)\cos kx}-1\right). \tag{7.19}$$

For each value of k, $\phi(x,k)$ has zero mean, and (7.19) is identical with the exact solution (7.15) for $k = (2k-m)/k$. Substituting (7.19) into (7.17), we compute

$$F[\phi] = -kh^2+2(2k-m)h-(3k-2m). \tag{7.20}$$

The right-hand side of (7.20) has a maximum at $h = (2k-m)/k$. It follows that the steady periodic solutions (7.15) are unstable.

8. The collapse of a strongly concentrated vortex stretched by a uniform plane strain

The asymptotic theory of §6 describes only the initial stages of the collapse process, in which the vortices may be approximated by vortex sheets slightly deformed from the horizontal. As we see from figure 4, the collapsing vortices ultimately become highly concentrated and nearly circular. We present an asymptotic theory that describes the collapse of a highly concentrated, nearly circular vortex of circulation Γ which is stretched by a uniform plane strain γ.

Table 3 indicates the appropriate units of the variables for this analysis. The choice of $(\nu/\gamma)^{\frac{1}{2}}$ as the lengthscale gives a balance between diffusive and convective vorticity fluxes. The units of vorticity ω and vortex-induced velocity $\boldsymbol{u}$ follow directly from the facts that the vortex has circulation Γ and core radius $(\nu/\gamma)^{\frac{1}{2}}$. The radical component

$$\omega^0(r,t) \equiv \int_0^{2\pi} \omega(r,\theta,t)\,\mathrm{d}\theta$$

of the vorticity distribution undergoes significant relative changes in time $1/\gamma$. This fixes $1/\gamma$ as the unit of time. In the units of table 3, the vorticity equation (3.3) reads

$$\omega_t + \nabla\cdot((Re''\,\boldsymbol{u}-y\hat{\boldsymbol{y}})\,\omega) = \Delta\omega, \tag{8.1}$$

$$Re'' = \frac{\Gamma}{\nu} \tag{8.2}$$

is the Reynolds number of the vortex.

At high Reynolds numbers, it is possible to have a vortex which is nearly axisymmetric. The compression from the strain induces only a slight deformation if the vortex is strong. Accordingly, we seek the vorticity distribution in the form

$$\omega = \omega^0(r,t)+\frac{1}{Re''}\omega^1(r,\theta,t,Re''), \tag{8.3}$$

where (r,θ) are polar coordinates of the plane and $\int_0^{2\pi}\omega^1(r,\theta,t,Re'')\,\mathrm{d}\theta = 0$. The vortex-induced velocity corresponding to (8.3) has the form

$$\boldsymbol{u} = \left(\frac{1}{r}\int_0^r r'\omega^0(r',t)\,\mathrm{d}r'\right)\hat{\boldsymbol{\theta}} + \frac{1}{Re''}\boldsymbol{u}^1(r,\theta,t,Re''). \tag{8.4}$$

The leading term in (8.4) is the tangential velocity field generated by the axisymmetric component $\omega^0(r,t)$ of the vorticity distribution.

We derive an evolution equation for $\omega^0(r,t)$. We substitute (8.3) and (8.4) into the vorticity equation (8.1) and integrate the resulting expression over the disk of radius r. We obtain

$$\int_0^r r'\omega_t^0(r',t)\,\mathrm{d}r' + F(r,t) = \int_0^r (r'\omega_r^0(r',t))_r\,\mathrm{d}r', \tag{8.5}$$

where

$$\begin{aligned} F(r,t) &\equiv \frac{1}{2\pi}\int_{|x|<r} \nabla\cdot((Re''\boldsymbol{u} - y\hat{\boldsymbol{y}})\,\omega\,\mathrm{d}\boldsymbol{x} \\ &= \frac{r}{2\pi}\int_0^{2\pi}(Re''\boldsymbol{u}'\cdot\hat{\boldsymbol{n}} - y\hat{\boldsymbol{y}}\cdot\hat{\boldsymbol{n}})\left(\omega^0 + \frac{1}{Re''}\omega^1\right)\mathrm{d}\theta. \end{aligned} \tag{8.6}$$

Here $\hat{\boldsymbol{n}} = \cos\theta\,\hat{\boldsymbol{x}} + \sin\theta\,\hat{\boldsymbol{y}}$ is the unit normal of the circle about the origin with radius r. We applied the divergence theorem to obtain the second line of (8.6) from the first. The vortex-induced velocity $\boldsymbol{u}$ is divergence-free. Hence $\int_0^{2\pi}\boldsymbol{u}^1(r,\theta,t,Re'')\cdot\hat{\boldsymbol{n}}\,\mathrm{d}\theta = 0$, and the expression for F reduces to

$$F = -r^2\omega^0\frac{1}{2\pi}\int_0^{2\pi}\sin^2\theta\,\mathrm{d}\theta + O\left(\frac{1}{Re''}\right) = -\tfrac{1}{2}r^2\omega^0 + O\left(\frac{1}{Re''}\right). \tag{8.7}$$

Here we set $y = r\sin\theta$ and $\hat{\boldsymbol{y}}\cdot\hat{\boldsymbol{n}} = \sin\theta$ to obtain this result. Substituting the value (8.7) for F into (8.5) and differentiating the result with respect to r, we obtain the equation for $\omega^0(r,t)$:

$$\omega_t^0 - \frac{1}{2r}(r^2\omega^0)_r = \frac{1}{r}(r\omega_r^0)_r + O\left(\frac{1}{Re''}\right). \tag{8.8}$$

To leading order (8.8) is identical with the equation governing an axisymmetric vortex which is stretched by a uniform axisymmetric strain (Batchelor 1967).

Equation (8.8) possesses a family of similarity solutions, given by

$$\omega = \frac{1}{4\pi a^2}\mathrm{e}^{-r^2/4a^2}, \quad a^2 \equiv 1 + (a_0^2 - 1)\,\mathrm{e}^{-t}, \tag{8.9}$$

where a_0 is an arbitrary positive constant. On restoring the original dimensional variables, this solution reads

$$\left.\begin{aligned} \omega &= \frac{r}{4\pi R^2(t)}\mathrm{e}^{-r^2/4R^2(t)}, \\ R^2(t) &\equiv \frac{\nu}{\gamma} + \left(R_0^2 + \frac{\nu}{\gamma}\right)\mathrm{e}^{-t/\gamma}. \end{aligned}\right\} \tag{8.10}$$

Equations (8.10) represent a columnar vortex with a Gaussian distribution of vorticity in its core. The core radius $R(t)$ decays exponentially from its initial value R^0 to its equilibrium value $(\nu/\gamma)^{\frac{1}{2}}$, which is the core radius of the well-known steady Burger's vortex.

Appendix A. Evaluation of $U[\sigma]$

We show that

$$U[\sigma] \equiv -\frac{1}{4\pi}\int_{-\infty}^{\infty} \frac{\hat{\sigma}-\hat{\sigma}'}{(x-x')^2}\sigma'\,\mathrm{d}x' = \tfrac{1}{4}\sigma\sigma_x. \tag{A 1}$$

Assume that $\sigma(x)$ has a Fourier integral representation

$$\sigma(x) = \int_{-\infty}^{\infty} s(k)\,\mathrm{e}^{\mathrm{i}kx}\,\mathrm{d}k. \tag{A 2}$$

We interpret the Fourier integral as a sum

$$\left.\begin{aligned} &\sigma(x) = \sigma^+(x)+\sigma^-(x), \\ &\sigma^+(x) \equiv \int_0^{\infty} s(k)\,\mathrm{e}^{\mathrm{i}kx}\,\mathrm{d}k, \quad \sigma^-(x) \equiv \int_{-\infty}^{0} s(k)\,\mathrm{e}^{\mathrm{i}kx}\,\mathrm{d}k. \end{aligned}\right\} \tag{A 3}$$

$\sigma^{\pm}(x)$ are analytic functions of x in the upper and lower half-planes respectively. $\sigma^{\pm}(x)\to 0$ as $\operatorname{Im} x\to \pm\infty$. Given the representation (A 3) of σ as the sum of upper and lower analytic functions $\sigma^+(x)$ and $\sigma^-(x)$, we find by use of the residue theorem that the Hilbert transform of $\sigma(x)$ is given by

$$\hat{\sigma}(x) = \frac{1}{\pi}\int_{-\infty}^{\infty} \frac{\sigma(x')}{x-x'}\mathrm{d}x' = -\mathrm{i}(\sigma^+(x)-\sigma^-(x)). \tag{A 4}$$

Substituting into (A 1) the value of $\hat{\sigma}(x)$ given in (A 3), we find

$$U = \frac{-\mathrm{i}}{4\pi}\int_{-\infty}^{\infty} \left\{\frac{\sigma^{+\prime}-\sigma^+}{(x'-x)^2}\sigma^{+\prime} - \frac{\sigma^{-\prime}-\sigma^-}{(x'-x)^2}\sigma^{-\prime} + \sigma^- \frac{\sigma^{+\prime}-\sigma^+}{(x'-x)^2} - \sigma^+\frac{\sigma^{-\prime}-\sigma^-}{(x'-x)^2}\right\}\mathrm{d}x'. \tag{A 5}$$

We apply the residue theorem to each of the terms on the right-hand side of (A 5) to obtain

$$\begin{aligned} U &= \tfrac{1}{4}(\sigma^+\sigma_x^+ + \sigma_x^-\sigma^- + \sigma^-\sigma_x^+ + \sigma^+\sigma_x^-) \\ &= \tfrac{1}{8}(\sigma^{+2}+\sigma^{-2}+2\sigma^+\sigma^-)_x = \tfrac{1}{8}((\sigma^+ + \sigma^-)^2)_x \\ &= \tfrac{1}{8}(\sigma^2)_x = \tfrac{1}{4}\sigma\sigma_x. \end{aligned} \tag{A 6}$$

Appendix B. Asymptotic evaluation of vortex-induced velocities

We show how the asymptotic expansions (6.7) and (6.8) of the integrals (6.2) and (6.3) are derived. We demonstrate the technique on (6.2). Equation (6.2) can be written as

$$u = -\int_{-\infty}^{\infty} \frac{1}{2\pi}\int_{-\infty}^{\infty} \frac{\epsilon\mu(y-y')\,(w^+ + w^-)\,\mathrm{d}x'}{(x'-x+\mathrm{i}\epsilon\mu\,|\,y-y'\,|)\,(x'-x-\mathrm{i}\epsilon\mu\,|\,y-y'\,|)}\mathrm{d}y', \tag{B 1}$$

where $\omega^+(x',y',t)+\omega^-(x',y',t)$ is the decomposition of ω into components $\omega^{\pm}$ that are analytic in the upper and lower halves of the x' plane with $\omega^{\pm}\to 0$ as $\operatorname{Im} x'\to\pm\infty$. Evaluating the residues at the poles $x' = x\pm\mathrm{i}\epsilon\mu\,|\,y-y'\,|$ of the integrand in (B 1) gives

$$u = -\frac{1}{2}\int_{-\infty}^{\infty} \operatorname{sgn}(y-y')\,\{w^+(x+\mathrm{i}\epsilon\mu\,|\,y-y'\,|, y', t)+\omega^-(x-\mathrm{i}\epsilon\mu\,|\,y-y'\,|, y', t)\}\,\mathrm{d}y'. \tag{B 2}$$

Expanding the integrand of (B 2) in powers of ϵ gives

$$u \sim -\frac{1}{2}\int_{-\infty}^{\infty} \{\operatorname{sgn}(y-y')(\omega^{+\prime}+\omega^{-\prime}) + \mathrm{i}\epsilon\mu(y-y')(\omega^{+\prime}-\omega^{-\prime})_x - \tfrac{1}{2}\epsilon^2\mu^2 \operatorname{sgn}(y-y')(y-y')^2(\omega^{+\prime}+\omega^{-\prime})_{xx}+\ldots\}\,\mathrm{d}y'. \quad \text{(B 3)}$$

Here $\omega^{\pm\prime}$ denotes $\omega^{\pm}(x,y',t)$. In (B 3) the sum $\omega^{+\prime}+\omega^{-\prime}$ is just ω'. The difference $\omega^{+\prime}-\omega^{-\prime}$ is related to ω by

$$\omega^+(x,y,t)-\omega^-(x,y,t) = \frac{1}{\pi\mathrm{i}}\int_{-\infty}^{\infty}\frac{\omega^+(x',y,t)+\omega^-(x',y,t)}{x'-x}\,\mathrm{d}x' = \mathrm{i}\frac{1}{\pi}\int_{-\infty}^{\infty}\frac{\omega(x',y,t)}{x-x'}\,\mathrm{d}x' = \mathrm{i}\hat{\omega}(x,y,t). \quad \text{(B 4)}$$

Hence (B 3) becomes

$$u \sim -\frac{1}{2}\int_{-\infty}^{\infty}\{\operatorname{sgn}(y-y')\,\omega' - \epsilon\mu(y-y')\,\hat{\omega}_{x'} - \tfrac{1}{2}\epsilon^2\mu^2\operatorname{sgn}(y-y')(y-y')^2\omega'_{xx}+\ldots\}\,\mathrm{d}y, \quad \text{(B 5)}$$

which is the result (6.7).

Appendix C. The flux of vorticity due to spanwise velocity

In (6.17) we found that to leading order the flux of vorticity due to spanwise velocity is given by

$$F^0 = \tfrac{1}{2}\mu\int_{-\infty}^{\infty}\int_{-\infty}^{\infty}(y-y')\,\hat{\omega}^{0\prime}_x\,\omega^0\,\mathrm{d}y'\,\mathrm{d}y, \quad \text{(C 1)}$$

where

$$\omega^0 = \frac{\sigma}{(2\pi)^{\frac{1}{2}}}\exp\left[-\frac{1}{2}\left(y-\frac{\hat{\sigma}}{2\mu}\right)^2\right] \quad \text{(C 2)}$$

is the leading-order vorticity distribution. We substitute (C 2) into (C 1) and evaluate F^0 as a functional of σ. We obtain

$$F^0 = \tfrac{1}{4}\sigma(\tfrac{1}{2}\hat{\sigma}^2 - \widehat{\sigma\hat{\sigma}})_x. \quad \text{(C 3)}$$

To evaluate the right-hand side of (C 3) we use the decomposition $\sigma = \sigma^+ + \sigma^-$, where $\sigma^\pm$ are analytic in the upper and lower halves of the x' plane, with $\sigma^\pm \to 0$ as $\operatorname{Im} x' \to \pm\infty$. Using the property $\sigma^+ - \sigma^- = \mathrm{i}\hat{\sigma}$, we find

$$\tfrac{1}{2}\hat{\sigma}^2 - \widehat{\sigma\hat{\sigma}} = -\tfrac{1}{2}(\sigma^+-\sigma^-)^2 + \sigma^{+2} + \sigma^{-2} = \tfrac{1}{2}(\sigma^+ + \sigma^-)^2 = \tfrac{1}{2}\sigma^2. \quad \text{(C 4)}$$

Hence (C 3) becomes

$$F^0 = \tfrac{1}{4}\sigma^2\sigma_x, \quad \text{(C 5)}$$

which is the result stated in (6.18).

REFERENCES

Batchelor, G. K. 1967 *An Introduction to Fluid Mechanics*, pp. 272–273. Cambridge University Press.

Benjamin, T. B. 1967 Internal waves of permanent form in fluids of great depth. *J. Fluid Mech.* **29**, 559–592.

Browand, F. K. & Weidman, P. D. 1976 Large scales in the developing mixing layer. *J. Fluid Mech.* **76**, 127–144.

Browand, F. K. & Winant, C. D. 1974 Vortex pairing: a mechanism of turbulent mixing layer growth at moderate Reynolds number. *J. Fluid Mech.* **63**, 237–255.

BROWN, G. & ROSHKO, A. 1974 On the density effects and large structure in turbulent mixing layers. *J. Fluid Mech.* **64**, 775–816.

CORCOS, G. & LIN, S. 1984 The mixing layer: deterministic models of a turbulent flow. Part 2. The origin of the three-dimensional motion. *J. Fluid Mech.* **139**, 67–95.

CORCOS, G. & SHERMAN, F. 1984 The mixing layer: deterministic models of a turbulent flow. Part 1. Introduction and the two-dimensional flow. *J. Fluid Mech.* **139**, 29–65.

LAMB, H. 1932 *Hydrodynamics*, 6th edn, pp. 232–233. Cambridge University Press.

LIN, S. J. & CORCOS, G. 1984 The mixing layer: deterministic models of a turbulent flow. Part 3. The effect of plain strain on the dynamics of streamwise vortices. *J. Fluid Mech.* **141**, 139–178.

ROSHKO, A. 1976 Structure of turbulent shear flows: a new look. *AIAA J.* **14**, 1349–1357.

SAFFMAN, P. & BAKER, G. 1979 Vortex interactions. *Ann. Rev. Fluid Mech.* **11**, 95–122.